Chemistry–A European Journal
Research Article
doi.org/10.1002/chem.202300577
Chemistry Europe
European Chemical Societies Publishing
www.chemeurj.org

# Understanding the Reactivity of Diazaborinines towards the Activation of σ-Bonds

Susana Portela[a] and Israel Fernández*[a]

**Abstract:** The poorly understood factors governing the small molecule activation reactions mediated by diazaborinines have been computationally explored in detail using quantum chemical tools. To this end, the activation of E–H σ-bonds (E = H, C, Si, N, P, O, S) has been investigated. These reactions, which proceed in a concerted manner, are exergonic and, in general, associated with relatively low activation barriers. In addition, the barrier becomes lower for the E–H bonds involving the heavier element in the same group ($\Delta G^{\neq}$: C > Si; N > P; O > S). This reactivity trend together with the mode of action of the diazaborinine system are quantitatively analyzed by means of the activation strain model of reactivity in combination with the energy decomposition analysis method.

## Introduction

The conversion of small molecules such as dihydrogen, carbon dioxide, nitrogen, ammonia, or methane into value-added species typically requires a bond activation step, which has been traditionally achieved using transition metal complexes.[1] Despite that, the use of main-group compounds has emerged in recent years as a useful alternative to activate strong chemical bonds[2] mainly due to the lower toxicity and cost of these species as compared to most of the commonly used transition metal complexes. In this regard, singlet-carbenes[3] together with their group 13 and group 14 analogues[4] as well as frustrated Lewis pairs (FLPs),[5] where the cooperative action of the Lewis antagonists facilitates the bond activation, should be especially highlighted.

Recently, alternative systems based on doubly boron-doped (hetero)arenes have been reported independently by the groups of Wagner,[6] Harmann[7] and Kinjo[8] (Figure 1). These species, which feature an aromatic 1,4-diborinine ring, are proven to achieve relatively facile activation of E–H σ-bonds (E = H, B, C, Si, N, P, O, S…).[9] Whereas the bond activation involving the diboraanthracene systems has been the focus of recent experimental and computational studies,[10] the mode of action of Kinjo's diazoborinines (Figure 1b) remains unclear so far. It was postulated that although the two boron atoms are equivalent in these species, they show an ambiphilic (i.e., nucleophilic/electrophile) nature, even featuring a B(I)/B(III) mixed-valence character,[8a,b] which would resemble the mode of action of FLPs. The current lack of understanding of how these main-group species actually activate σ-bonds severely hampers future developments to produce more active systems, which prompted us to carry out a detailed exploration of the factors controlling the reactivity of these highly useful compounds.

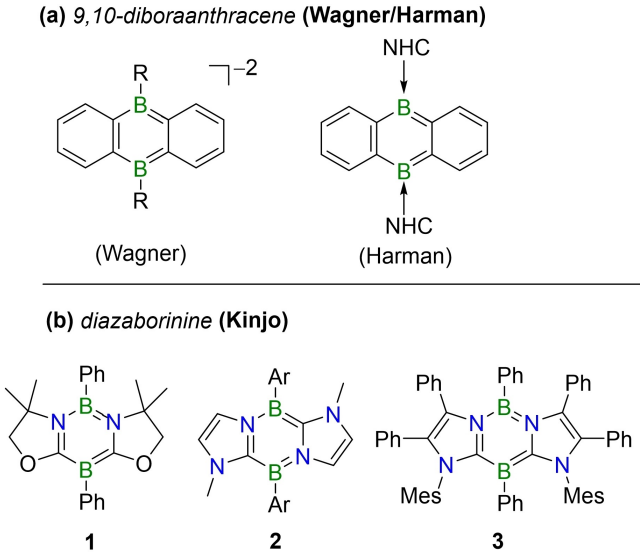


**Figure 1.** Representative 1,4-diborinines described recently.

To this end, the mode of action and reactivity trends involving these diazaborinines shall be analyzed quantitatively in detail through the application of the activation strain model (ASM) of reactivity[11] in combination with the energy decomposition analysis (EDA) method.[12] This ASM-EDA approach was selected because it has greatly contributed to our current understanding of fundamental transformations in chemistry,[13] and particularly, of the mode of action and cooperativity of FLPs[14,15] and related main-group species.[16] In addition, other

[a] S. Portela, Prof. Dr. I. Fernández
Departamento de Química Orgánica y Centro de Innovación en Química Avanzada (ORFEO-CINQA)
Facultad de Ciencias Químicas, Universidad Complutense de Madrid
Ciudad Universitaria, 28040-Madrid (Spain)
E-mail: israel@quim.ucm.es

Supporting information for this article is available on the WWW under https://doi.org/10.1002/chem.202300577

issues such as the role of aromaticity of the diazoborinine on the reactivity will be explored as well.

## Results and Discussion

We first explored the dihydrogen activation mediated by diazaborinines **1**–**3** as one of the most representative bond activation reactions. Experimentally, it was found that diazaborinines **2** and **3** readily cleave the H–H σ-bond with concomitant formation of two new B–H bonds leading to the formation of the corresponding *cis*-adduct (i.e., both H atoms are placed at the same side of the $B_2C_2N_2$ six-membered ring). Moreover, whereas **3** produces the adduct upon heating in benzene at 70 °C in 5 h, 1,3,2,4-diazaborinine **2** produces the analogous adduct upon heating in toluene at 90 °C for 36 h, which indicates that **3** is more reactive than **2** towards the dihydrogen activation. In contrast, no H–H activation has been reported involving diazaborinine **1**.

Our calculations (Figure 2) suggest that the dihydrogen splitting occurs in a concerted manner leading to the corresponding adducts (**1-3-H2**) through the respective cyclic transition state **TS**. These saddle points are therefore associated with the rupture of the H–H bond with the concomitant formation of both B–H bonds. Moreover, the process begins with the formation of an initial weakly bonded van der Waals reactant complex (**RC-H2**), which, in all cases, lies approximately 2–3 kcal/mol (average value) below the separate reactants. However, the formation of these species becomes endergonic (ca. 3 kcal/mol) when thermal free-energy corrections at 298.15 K are included and for this reason, these species are not shown in the profile of Figure 2.

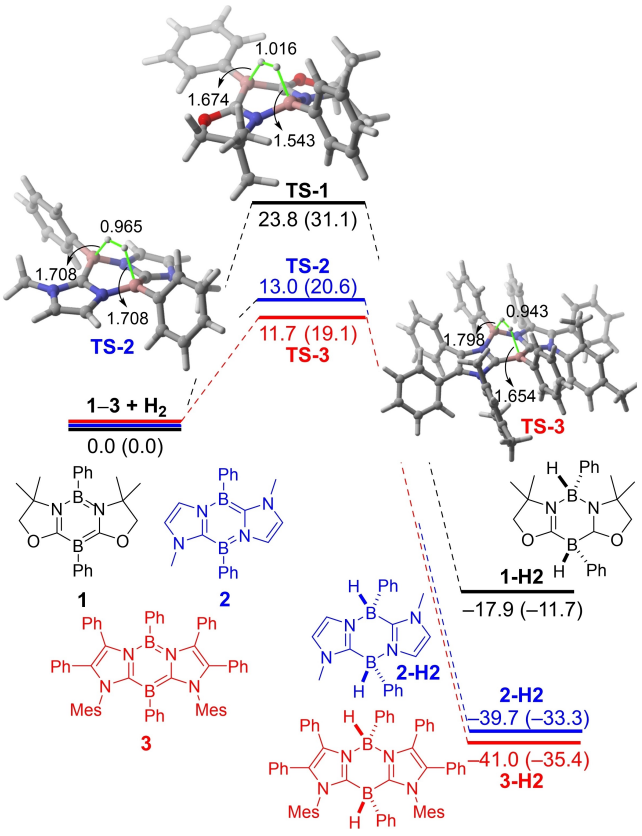


**Figure 2.** Computed reaction profiles for the $H_2$ activation reactions promoted by diazaborinines **1**–**3**. Relative electronic (Δ*E*) and free (Δ*G*, within parentheses) energies and bond distances are given in kcal/mol and angstroms, respectively. All data have been computed at the PCM(benzene)-M06-2X/def2-TZVPP//PCM(benzene)-B3LYP-D3/def2-SVP level.

Before analyzing the origin of the different reactivity of diazaborinines **1**–**3**, we first explored how the activation of σ-H–H bond actually takes place. To this end, we focused on the process mediated by species **2** and applied the EDA-NOCV (Natural Orbital for Chemical Valence)[17] method to not only identify the nature of the molecular orbitals involved in the dihydrogen activation but also to quantify their relative contribution. Figure 3 shows snapshots of the corresponding NOCV deformation densities at three key points (reactant complex, midpoint, and **TS**) along the reaction coordinate (rather similar plots are found for the rest of the studied systems). Note that at the very early stage of the reaction (at a B···H bond-forming distance of 2.81 Å), the principal charge depletion region (in red) belongs to a π-molecular orbital centered at the diazaborinine ring (which corresponds to the HOMO of **2**) whereas the charge accumulation (in blue) corresponds to the empty σ*(H–H) molecular orbital. Therefore, at the beginning of the process the only measurable orbital interaction between **2** and $H_2$ corresponds to the π-HOMO(**2**)→σ*(H–H) interaction (associated stabilization energy, $\Delta E(\varrho_1)$, of −2.1 kcal/mol). Moving forward along the reaction coordinate, this charge transfer process continuously reinforces and dominates up to the transition state region, where $\Delta E(\varrho_1) = -29.5$ kcal/mol. Interestingly, at the midpoint (r(B···H) = 2.15 Å) the reverse charge flow (denoted as $\varrho_2$) involving the donation from the doubly occupied σ(H–H) molecular orbital to the vacant π*-molecular orbital of **2** (which corresponds to the LUMO), starts to appear and becomes clearly developed at the transition state. According to the computed associated energies, it becomes evident that the π-HOMO(**2**)→σ*(H–H) interaction dominates over the σ(H–H)→π*-LUMO(**2**) interaction along the entire reaction coordinate. Therefore, our NOCV calculations indicate that both orbital interactions take place along the reaction path but at different stages, that is, not simultaneously becoming the π-HOMO(**2**)→σ*(H–H) most emphasized at the beginning of the process and responsible for the polarization of the σ(H–H) bond, thus allowing the σ(H–H)→π*-LUMO(**2**) interaction to occur. This asynchronous $H_2$ activation mode resembles that found by us in the analogous transformation promoted by group15/group13 geminal FLPs.[14a,c] However, in sharp contrast, the dominant interaction in the FLP-mediated activation comes from the σ(H–H)→$p_z$(Lewis acid) interaction, which polarizes the H–H bond allowing the interaction with the σ*(H–H) molecular orbital (by the lone-pair of the base) to take place. Therefore, our results confirm that the mode of activation of $H_2$ by diazaborinines resembles that of FLPs but, at variance, the donation to the σ*(H–H) molecular orbital becomes the dominant interaction along the entire reaction coordinate.

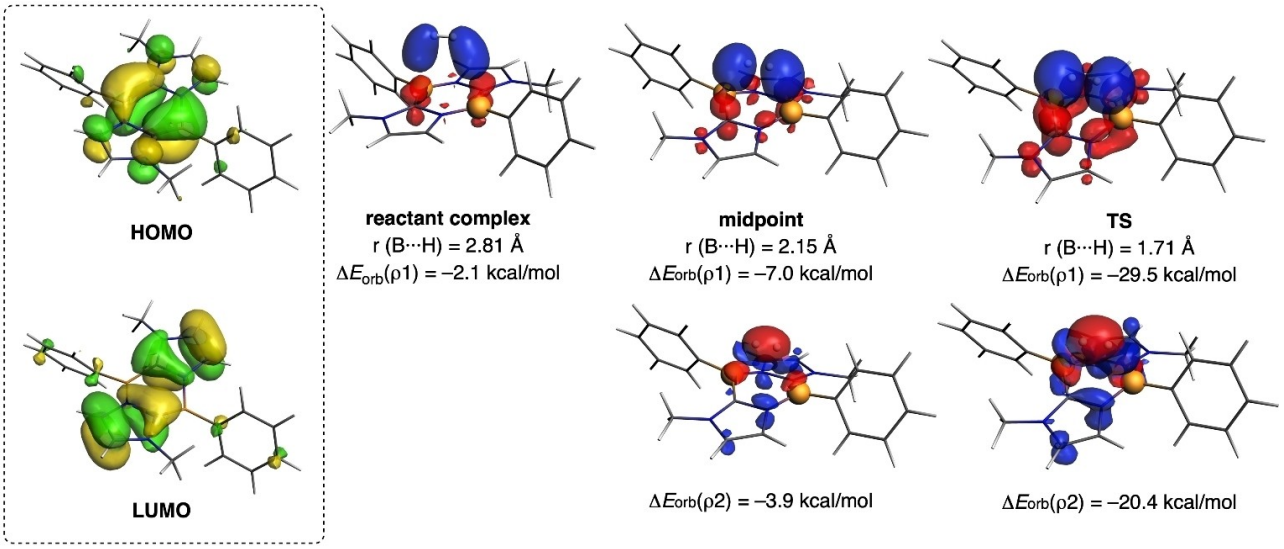


**Figure 3.** Contour plots of the NOCV deformation densities ϱ (isosurface value of 0.001 a.u.) and the associated energies $\Delta E(\varrho)$ for the main orbital interactions between diazaborinine **2** and $H_2$ in selected points along the reaction coordinate. The electronic charge flows from red to blue. All data were computed at the ZORA-B3LYP-D3/TZ2P//PCM(benzene)-B3LYP-D3/def2-SVP level. Inset: Frontier molecular orbitals of compound **2**.

Once the mode of activation has been explored, we then turned our attention to the factors governing the different reactivity of diazaborinines **1**–**3**. From the data in Figure 2, it becomes evident that species **1** is clearly less reactive, from both kinetic and thermodynamic points of view, than compounds **2** or **3**, which agrees with the lack of experimental evidence for the activation of $H_2$ promoted by **1**. In addition, our calculations also suggest that diazaborinie **3** is more reactive than **2**, which is also consistent with the experimental findings (see above). Interestingly, the computed barriers and reaction energies nicely correlate with the H···H bond-breaking distance in the corresponding transition states in the sense that longer distances (i.e. later transition states) are associated with a higher barrier and less exergonic transformation, which fully agrees with the Hammond-Leffer postulate.[18]

When comparing the reaction involving **1** with the analogous process involving **2** (or **3**), one immediately realizes that in the later transformation, there occurs a substantial gain in aromaticity in the two imidazole rings of the corresponding adduct. As this is not possible in the **1-H2** adduct, this gain in aromaticity should be, at least in part, responsible for the much higher exergonicity (and reactivity) computed for the $H_2$-activation mediated by **2** (and **3**) as compared to **1**. To check this hypothesis, we explore the variation of the aromaticity along the reaction coordinate for the processes mediated by **1** and **2** by computing the corresponding Nuclear Independent Chemical Shift (NICS)[19] values and using the Anisotropy of the Induced Current Density (AICD)[20] method. As shown in Figure 4, whereas the initial aromaticity of the central 6π electrons diazaborinine ring in **1** ($NICS(1)_{zz} \approx -9.5$ ppm) vanishes along the reaction coordinate as a consequence of the formation of the new two B–H bonds, the non-aromatic nature of the adjacent five-membered rings remains practically unaltered ($NICS(1)_{zz} \approx -2$ ppm). Therefore, there is a net decrease in the aromaticity of the system during the $H_2$-activation reaction. At variance, diazoborinine **2** features a clear 14π electron macrocyclic diatropic ring current which is responsible for the high $NICS(1)_{zz}$ values computed for the three fused rings. The $H_2$-activation provokes that this macrocyclic ring current transforms into two distinct 6π electrons diatropic currents localized in the imidazole rings, which is confirmed by a clear increase in the corresponding $NICS(1)_{zz}$ values (see Figure 4). This aromaticity gain, which derives from the occurrence of two Clar-sextets in the final adducts,[21] is translated into a significant thermodynamic stability which is finally reflected in the higher exergonicity computed for this process as compared to that involving **1**. Despite that, there exists no straightforward, causal physical relationship between these magnetic indicators of aromaticity and the ultimate factors controlling the barrier height of the process.

For this reason, we applied the activation strain model (ASM) of reactivity to gain quantitative insight into the factors controlling the different reactivity of these diazoborinines. Figure 5 shows the computed activation strain diagrams (ASDs) for the $H_2$ activation reactions promoted by compounds **1**–**3** from the initial stages of the transformations to the respective transition states and projected onto the shortest B···H bond-forming distance. From the data in Figure 5, it becomes clear that the reduced reactivity of diazaborinine **1** results mainly from a more destabilizing strain energy along practically the entire reaction coordinate and also, albeit to a lesser extent, from a less stabilizing interaction energy between the increasingly deformed reactants. At variance, the reactions involving diazaborinines **2** and **3** benefit from a much lower strain energy which results in the computed lower barriers. The enhanced reactivity of species **3** over **2** derives not from the energy penalty required to deform the reactants as the $\Delta E_{strain}$ term is slightly more destabilizing for the process involving **3**, but

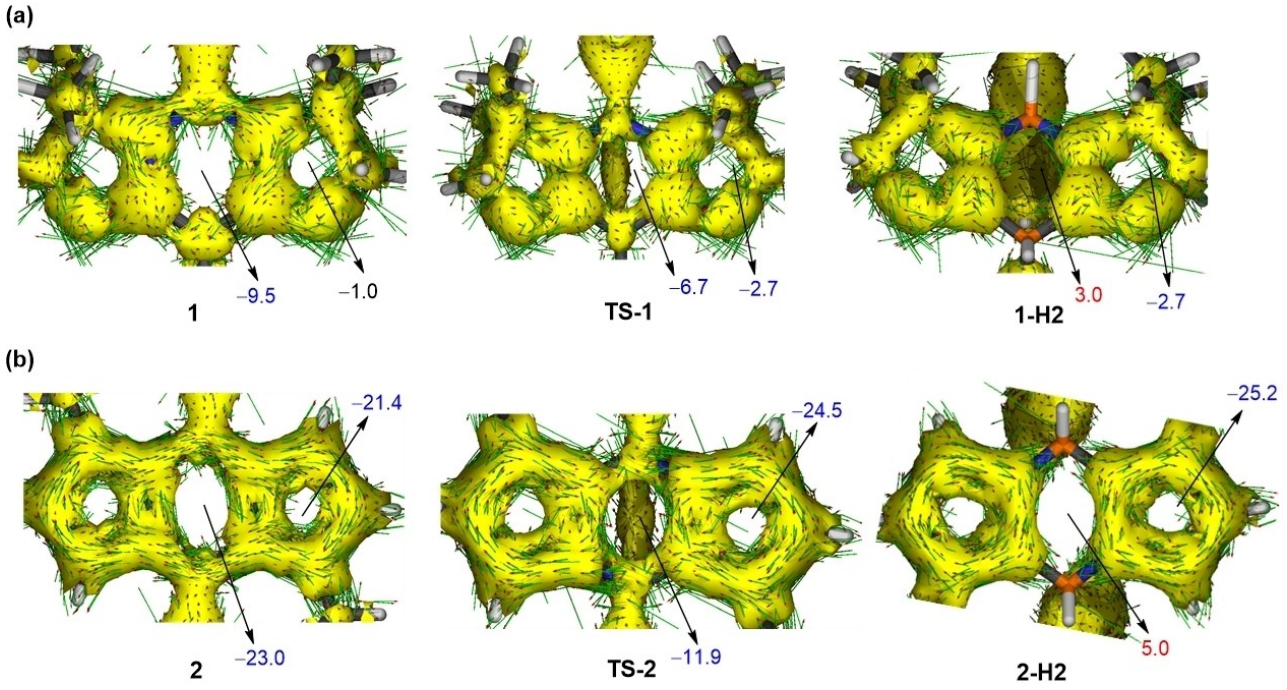


**Figure 4.** Computed ACID plots (isosurface value of 0.04) and NICS(1)$_{zz}$ values (in ppm) for the key points of the dihydrogen activation reaction mediated by diazaborinine **1** (a) and **2** (b).

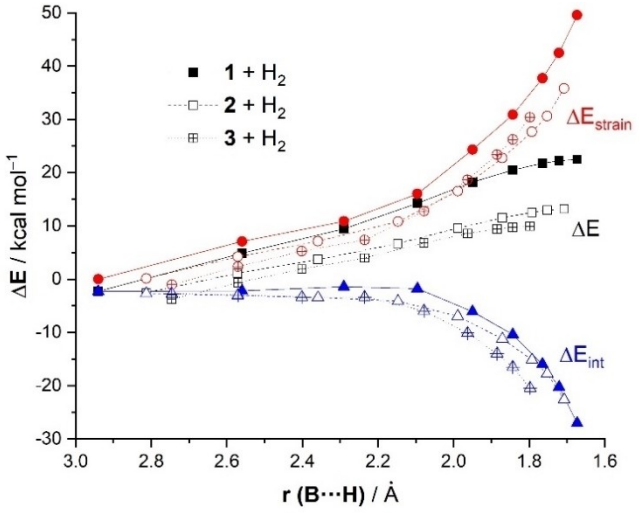


**Figure 5.** Comparative activation strain analyses of the dihydrogen activation reactions mediated by **1** (solid lines), **2** (dashes lines) and **3** (dotted lines) projected onto the shortest B···H bond-forming distance. All data have been computed at the PCM(benzene)-B3LYP-D3/def2-TZVPP//PCM(benzene)-B3LYP-D3/def2-SVP level.

exclusively from the interaction energy between the deformed reactants, which is clearly much stronger for the $H_2$-activation mediated by **3** along the entire reaction coordinate. For instance, at the same consistent B···H bond-forming distance of 1.82 Å,[22] although the difference in the strain energy slightly favors the reaction involving **2** ($\Delta\Delta E_{strain} = -2.3$ kcal/mol), the difference in the interaction energy is higher ($\Delta\Delta E_{int} = 4.8$ kcal/mol) therefore rendering the barrier for the process mediated by **3** lower.

The energy decomposition analysis (EDA) method was applied next to quantitatively understand the reasons behind the stronger interaction energy computed for the **3** + $H_2$ reaction, which results in a lower barrier as compared to the analogous process involving **2**. Figure 6 graphically shows the evolution of the EDA contributors along the reaction coordinate for both activation reactions once again from the initial stages of the transformation to the respective transition states and projected onto the shortest B···H bond-forming distance. From the data in Figure 6, it becomes clear that the process mediated by **2** benefits from a lower Pauli repulsion along the entire transformation. However, the more destabilizing $\Delta E_{Pauli}$ computed for the $H_2$-activation promoted by **3** is compensated by much stronger orbital interactions ($\Delta E_{orb}$) between the reactants and also, albeit to a much lesser extent, by stronger electrostatic attractions ($\Delta V_{elstat}$) between the deformed reactants, particularly, at the transition state region (i.e. where the barrier takes place). For instance, at the same consistent B···H bond forming distance of 1.82 Å,[22] the difference in the total Pauli repulsion, $\Delta\Delta E_{Pauli} = -12.9$ kcal/mol (favoring the **2** + $H_2$ reaction), is completely offset by the difference in the orbital interactions, $\Delta\Delta E_{orb} = 11.9$ kcal/mol together with the electrostatic attractions, $\Delta\Delta V_{elstat} = 4.6$ kcal/mol (favoring **3** + $H_2$). The stronger orbital interactions derive, according to the NOCV method, from both a stronger $\pi$-HOMO→$\sigma^*$(H–H) interaction ($\Delta\Delta E(\varrho_1) = 9.6$ kcal/mol) and also, albeit to a lesser extent, stronger $\sigma$(H–H)→$\pi^*$-LUMO interaction ($\Delta\Delta E(\varrho_2) = 1.4$ kcal/mol, computed at the same consistent B···H bond-forming distance

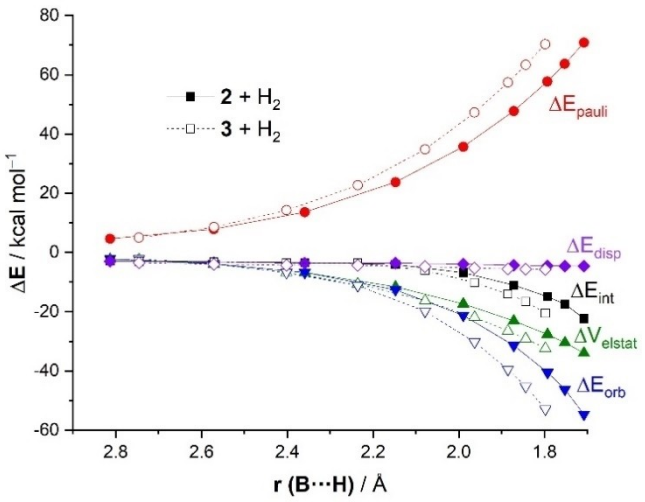


**Figure 6.** Comparative activation strain analyses of the dihydrogen activation reactions mediated by **2** (solid lines) and **3** (dashes lines) projected onto the shortest B···H bond-forming distance. All data have been computed at the ZORA-B3LYP-D3/TZ2P//PCM(benzene)-B3LYP-D3/def2-SVP level.

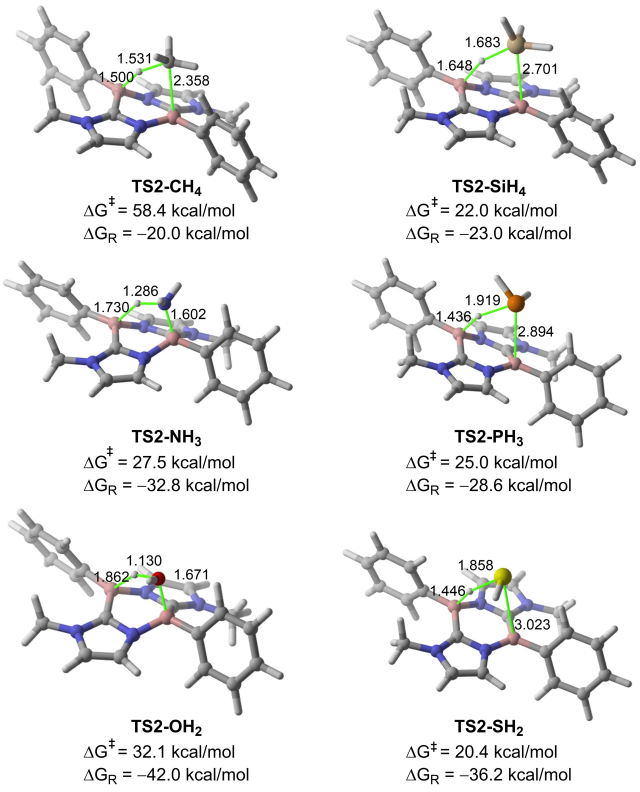


**Figure 7.** Optimized transition states for the small molecule activation reactions mediated by diazaborinine **2**. Free activation barriers ($\Delta G^{\neq}$) and reaction energies ($\Delta G_R$) were computed at the PCM(benzene)-M06-2X/def2-TZVPP//PCM(benzene)-B3LYP-D3/def2-SVP level.

of 1.82 Å). Therefore, it can be concluded that the enhanced reactivity of diazaborinine **3** as compared to **2** originates mainly from its higher donor (and acceptor, to a lesser extent) ability which results in a stronger interaction with the $H_2$ molecule and ultimately to the lower barrier computed for the $H_2$ splitting reaction.

### Activation of other E–H σ-bonds

Once the activation of dihydrogen has been investigated in detail, we then explored the activation of other σ-bonds including group 14 ($CH_4$, $SiH_4$), group 15 ($NH_3$ and $PH_3$) and group 16 ($H_2O$ and $SH_2$) species. Experimentally, it has been reported that diazoborinine **2** readily activates aryl silanes ($PhSiH_3$, $Ph_2SiH_2$) and arylphophines at room temperature,[8b] whereas the activation of $NH_3$ was reported by using diazaborinine **3** in 30 min at −50 °C,[8c] thus indicating the easiness of these activation reactions.

To enable a direct comparison, we focused on the activation reactions involving **2** and leading to the corresponding *cis*-adduct. We found that, similar to the dihydrogen activation reaction, in all cases the E–H σ-bond activation occurs in a concerted manner through the corresponding cyclic transition state which is associated with the splitting of the E–H bond with concomitant formation of the new B–H and B–E bonds (see Figure 7).

From the data gathered in Figure 7, all the considered E–H activation reactions are highly exergonic ($\Delta G_R$ ranging from −20 to −40 kcal/mol). According to the computed barrier heights, these transformations are predicted to be feasible at room temperature or upon moderate heating ($\Delta G^{\neq}$ ranging from 20.4 to 32.1 kcal/mol), which agrees with the available experimental data involving the facile activation of silanes, phosphines and ammonia (see above). In sharp contrast, similar to related $C_{sp3}$–H activation reactions mediated by other main-group systems,[16,23] the process involving methane proceeds with a rather high activation barrier ($\Delta G^{\neq} \approx 60$ kcal/mol), thus indicating that this particular activation reaction is unfeasible when mediated by diazaborinines.

Interestingly, in all cases an evident reactivity trend is revealed, namely the barrier becomes lower for the E–H bonds involving the heavier element in the same group ($\Delta G^{\neq}$: C > Si; N > P; O > S). To understand the reasons behind this reactivity trend, the ASM-EDA(NOCV) approach was applied again. Figure 8 shows the corresponding ASDs for the reactions involving $CH_4$ and $SiH_4$, as representative examples, from the initial stages of the transformation to the corresponding transition states and projected onto the B···H bond-forming distance. From the data in Figure 8, it becomes clear that the high barrier computed for the activation of methane mediated by **2** finds its origin in the rather high strain energy computed for this process (mainly deriving from the distortion of the $CH_4$ reactant) which compensates the stabilizing effect of the interaction between the deformed reactants. At variance, the energy required to deform the $SiH_4$ reactant is comparatively much lower and as result, the computed total $\Delta E_{strain}$ is clearly much less destabilizing, particularly at the transition state region. In addition, the **2** + $SiH_4$ reaction also benefits from a stronger interaction between the deformed reactants along the entire reaction

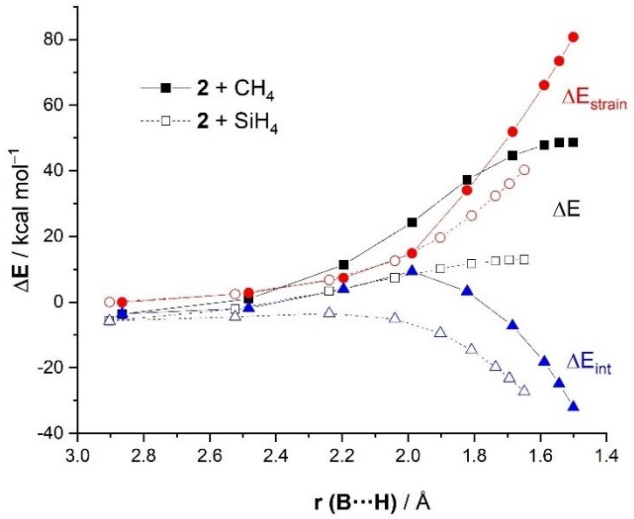


**Figure 8.** Comparative activation strain analyses of the $CH_4$ (solid lines) and $SiH_4$ (dashes lines) activation reactions mediated by diazaborinine **2** projected onto the B···H bond-forming distance. All data have been computed at the PCM(benzene)-B3LYP-D3/def2-TZVPP//PCM(benzene)-B3LYP-D3/def2-SVP level.

coordinate. Therefore, the combination of a lower strain with a more stabilizing interaction results in the lower barrier computed for the activation involving the heavier system.

The EDA(NOCV) method was used to understand the factors leading to the stronger interaction energy computed for the activation of $SiH_4$ in comparison to its lighter counterpart, $CH_4$. From the data in Figure 9, which shows the evolution of the EDA terms for both reactions along the reaction coordinate, the computed higher $\Delta E_{int}$ value derives mainly from stronger orbital interactions and, to a lesser extent, also from more stabilizing electrostatic attractions (the other terms, namely Pauli repulsion and dispersion interactions, are essentially identical for both activation reactions, particularly at the transition state region).

The NOCV extension of the EDA method once again indicates that two main orbital interactions dominate these activation reactions, namely the π-HOMO→σ*(E–H) interaction and the σ(E–H)→π*-LUMO interaction (denoted as $\varrho_1$ and $\varrho_2$, respectively, Figure 10). Similar to the related $H_2$ activation reaction, $\varrho_1 > \varrho_2$, therefore indicating that the donation from the π-HOMO of the diazaborinine dominates over the corresponding backdonation from the σ(E–H) molecular orbital. Interestingly, when comparing the values for the associated stabilization energies ($\Delta E(\varrho)$, computed at the same consistent B···H bond-forming distance of 1.68 Å),[22] it becomes clear that both molecular orbital interactions, and particularly $\varrho_1$, are stronger for the process involving $SiH_4$ as compared to the analogous reaction involving $CH_4$. This, therefore, indicates that the Si–H bond in $SiH_4$ is both a better acceptor and a better donor (albeit to a lesser extent) than the C–H bond in methane in their reactions with diazaborinine **2**. The higher strength of both molecular orbital interactions results in stronger total orbital interactions which ultimately constitutes the main factor leading to the computed stronger interaction between the deformed reactants for the activation of silane. This, together with the computed much lower strain energy required to deform the $SiH_4$ reactant, leads to the computed lower barrier for this process in comparison with the analogous activation reaction involving $CH_4$.

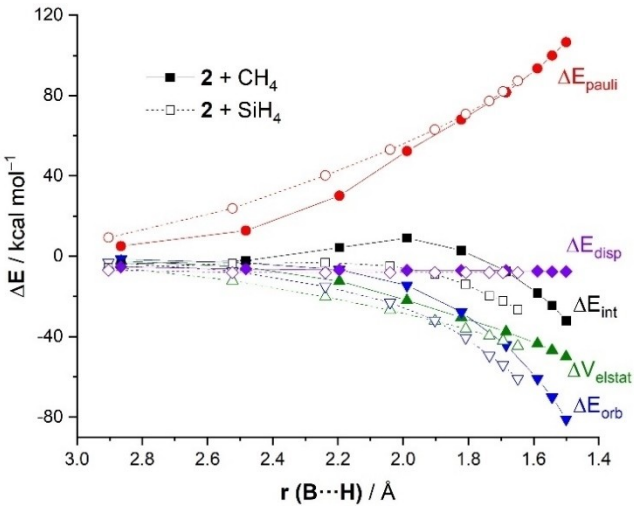


**Figure 9.** Comparative activation strain analyses of the $CH_4$ (solid lines) and $SiH_4$ (dashes lines) activation reactions mediated by diazaborinine **2** projected onto the B···H bond-forming distance. All data have been computed at the ZORA-B3LYP-D3/TZ2P//PCM(benzene)-B3LYP-D3/def2-SVP level.

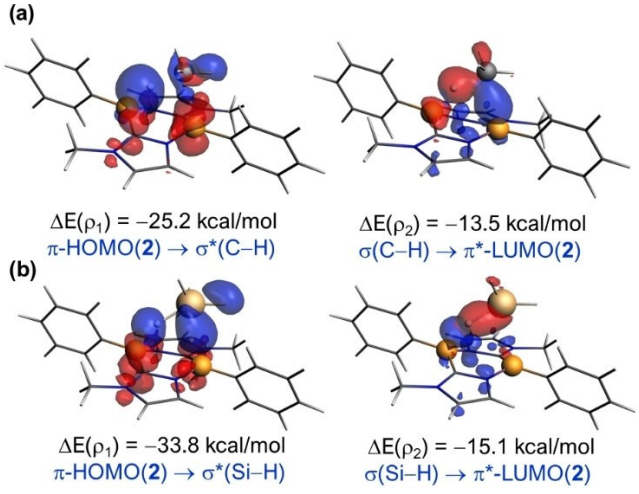


**Figure 10.** Contour plots of the NOCV deformation densities ϱ (isosurface value of 0.001 a.u.) and the associated energies $\Delta E(\varrho)$ for the main orbital interactions between diazaborinine **2** and $CH_4$ (a) and $SiH_4$ (b) at the same consistent B···H bond-forming distance of 1.68 Å. The electronic charge flows from red to blue. All data were computed at the ZORA-B3LYP-D3/TZ2P//PCM(benzene)-B3LYP-D3/def2-SVP level.

## Conclusion

From the computational study reported herein, it can be concluded that the activation reaction of E–H σ-bonds mediated by diazaborinines occurs in a concerted manner leading to the simultaneous E–H bond breaking and formation of new B–E and B–H bonds. These reactions are exergonic and, in general, associated with relatively low activation barriers (with the notable exception of the activation of $CH_4$). Although the process involves the loss of aromaticity of the 6π electron $B_2C_2N_2$ six-membered ring, it results in a net aromaticity gain in those cases where the borinine ring is flanked by two fused imidazole rings. According to the NOCV method, the main orbital interactions involved in the bond activation reaction take place along the reaction path at different stages, that is, not simultaneously becoming the donation from the π-HOMO(diazaborinine) to the σ*(E–H) molecular orbital most emphasized at the beginning of the process, which resembles the mode of activation of Frustrated Lewis Pairs. In addition, it is found that the activation barrier of this process becomes lower for the E–H bonds involving the heavier element in the same group ($\Delta G^{\neq}$: C > Si; N > P; O > S), which, in the representative case of the reactions involving $CH_4$ and $SiH_4$, derives mainly from a lower strain for the heavier reactant together with a stronger orbital interaction between the deformed reactants along the entire reaction coordinate.

## Computational Details

Geometry optimizations of the molecules were performed without symmetry constraints using the Gaussian09 (RevD.01) suite of programs[24] at the dispersion-corrected B3LYP[25]-D3[26]/def2-SVP[27] level including solvent effects (solvent = benzene) with the polarization continuum model (PCM) method.[28] Reactants and adducts were characterized by frequency calculations and have positive definite Hessian matrices. Transition states show only one negative eigenvalue in their diagonalized force constant matrices, and their associated eigenvectors were confirmed to correspond to the motion along the reaction coordinate under consideration using the Intrinsic Reaction Coordinate (IRC) method.[29] Energy refinements were carried out by means of single-point calculations at the accurate M06-2X[30] level using the much larger triple-ζ basis set def2-TZVPP.[27] This level is denoted PCM(benzene)-M06-2X/def2-TZVPP//PCM(benzene)-B3LYP-D3/def2-SVP.

The aromaticity of the considered species has been assessed by the computation of the nuclear independent chemical shift (NICS)[19] values using the gauge invariant atomic orbital (GIAO) method[31] at the B3LYP/def2-SVP//PCM(benzene)-B3LYP-D3/def2-SVP level. Ring currents were computed using the Anisotropy of the Induced Current Density (ACID) method.[20]

**Activation strain model of reactivity and energy decomposition analysis**: Within the ASM method,[11] also known as the distortion/interaction model,[11c] the potential energy surface $\Delta E(\zeta)$ is decomposed along the reaction coordinate, ζ, into two contributions, namely the strain $\Delta E_{strain}(\zeta)$ associated with the deformation (or distortion) required by the individual reactants during the process and the interaction $\Delta E_{int}(\zeta)$ between these increasingly deformed reactants [Eq. (1)]:

$$\Delta E(\zeta) = \Delta E_{strain}(\zeta) + \Delta E_{int}(\zeta) \quad (1)$$

Within the EDA method,[12] the interaction energy can be further decomposed into the following chemically meaningful terms [Eq. (2)]:

$$\Delta E_{int}(\zeta) = \Delta V_{elstat}(\zeta) + \Delta E_{Pauli}(\zeta) + \Delta E_{orb}(\zeta) + \Delta E_{disp}(\zeta) \quad (2)$$

The term $\Delta V_{elstat}$ corresponds to the classical electrostatic interaction between the unperturbed charge distributions of the deformed reactants and is usually attractive. The Pauli repulsion $\Delta E_{Pauli}$ comprises the destabilizing interactions between occupied orbitals and is responsible for any steric repulsion. The orbital interaction $\Delta E_{orb}$ accounts for bond pair formation, charge transfer (interaction between occupied orbitals on one moiety with unoccupied orbitals on the other, including HOMO-LUMO interactions), and polarization (empty-occupied orbital mixing on one fragment due to the presence of another fragment). Moreover, the NOCV (Natural Orbital for Chemical Valence)[17] extension of the EDA method has been also used to further partition the $\Delta E_{orb}$ term. The EDA-NOCV approach provides pairwise energy contributions for each pair of interacting orbitals to the total bond energy.

The program package ADF[32] was used for EDA calculations using the optimized PCM(benzene)-B3LYP-D3/def2-SVP geometries at the same B3LYP-D3 level in conjunction with a triple-ζ-quality basis set using uncontracted Slater-type orbitals (STOs) augmented by two sets of polarization functions with a frozen-core approximation for the core electrons.[33] Auxiliary sets of s, p, d, f, and g STOs were used to fit the molecular densities and to represent the Coulomb and exchange potentials accurately in each SCF cycle.[34] Scalar relativistic effects were incorporated by applying the zeroth-order regular approximation (ZORA).[35] This level of theory is denoted ZORA-B3LYP-D3/TZ2P//PCM(benzene)-B3LYP-D3/def2-SVP.

## *Acknowledgements*

This work was supported by the Spanish MCIN/AEI/10.13039/501100011033 (Grants PID2019-106184GB-I00 and RED2018-102387-T). S.P. acknowledges the MCIN for a FPI grant.

## Conflict of Interests

The authors declare no conflict of interest.

## Data Availability Statement

The data that support the findings of this study are available in the supplementary material of this article.

**Keywords:** activation · DFT calculations · diazaborinine · reactivity · small molecules

[1] See, for instance: a) J. F. Hartwig, in *Organotransition Metal Chemistry: From Bonding to Catalysis*, University Science Books, Mill Valley, CA, **2010**; b) M. Aresta, in *Carbon Dioxide as Chemical Feedstock*, Wiley-VCH, Weinheim, **2010**; c) B. M. Bhanage and M. Arai, in *Transformation and Utilization of Carbon Dioxide*, Springer-Verlag, Berlin, Heidelberg, **2014**;

d) X. Lu, in *Carbon Dioxide and Organometallics*, Springer International Publishing, Switzerland, **2016**; e) *Nitrogen Fixation; Topics in Organometallic Chemistry*, 60, ed. Y. Nishibayashi, Springer, **2017**.
[2] a) P. P. Power, *Nature* **2010**, *463*, 171–177; b) T. Chu, G. I. Nikonov, *Chem. Rev.* **2018**, *118*, 3608–3680.
[3] Representative examples: a) G. D. Frey, V. Lavallo, B. Donnadieu, W. W. Schoeller, G. Bertrand, *Science* **2007**, *316*, 439–441; b) D. Martin, M. Soleilhavoup, G. Bertrand, *Chem. Sci.* **2011**, *2*, 389–399; c) M. Soleilhavoup, G. Bertrand, *Acc. Chem. Res.* **2015**, *48*, 256–266; d) M. Melaimi, R. Jazzar, M. Soleilhavoup, G. Bertrand, *Angew. Chem. Int. Ed.* **2017**, *56*, 10046–10068; *Angew. Chem.* **2017**, *129*, 10180–10203.
[4] See, for instacne: a) M. Haaf, T. A. Schmedake, R. West, *Acc. Chem. Res.* **2000**, *33*, 704–714; b) C. Cui, H. W. Roesky, H.-G. Schmidt, M. Noltemeyer, H. Hao, F. Cimpoesu, *Angew. Chem. Int. Ed.* **2000**, *39*, 4274–4276; *Angew. Chem.* **2000**, *112*, 4444–4446; c) S. Yao, Y. Xiong, M. Driess, *Organometallics* **2011**, *30*, 1748–1767; d) T. Chu, I. Korobkov, G. I. Nikonov, *J. Am. Chem. Soc.* **2014**, *136*, 9195–9202; e) T. Chu, G. I. Nikonov, *Chem. Rev.* **2018**, *118*, 3608–3680.
[5] For leading reviews, see: a) D. W. Stephan, G. Erker, *Angew. Chem. Int. Ed.* **2010**, *49*, 46–76; *Angew. Chem.* **2010**, *122*, 50–81; b) G. Erker, *Pure Appl. Chem.* **2012**, *84*, 2203–2217; c) D. W. Stephan, G. Erker, *Top. Curr. Chem.* **2013**, *332*, *Frustrated Lewis Pairs I*; d) D. W. Stephan, G. Erker, *Chem. Sci.* **2014**, *5*, 2625–2641; e) D. W. Stephan, *J. Am. Chem. Soc.* **2015**, *137*, 10018–10032; f) D. W. Stephan, G. Erker, *Angew. Chem. Int. Ed.* **2015**, *54*, 6400–6441; *Angew. Chem.* **2015**, *127*, 6498–6541; g) D. W. Stephan, *Acc. Chem. Res.* **2015**, *48*, 306–316; h) D. W. Stephan, *Science* **2016**, *354*, aaf7229.
[6] a) A. Lorbach, M. Bolte, H.-W. Lerner, M. Wagner, *Organometallics* **2010**, *29*, 5762–5765; b) E. Januszewski, A. Lorbach, R. Grewal, M. Bolte, J. W. Bats, H.-W. Lerner, M. Wagner, *Chem. Eur. J.* **2011**, *17*, 12696–12705; c) E. von Grotthuss, M. Diefenbach, M. Bolte, H.-W. Lerner, M. C. Holthausen, M. Wagner, *Angew. Chem. Int. Ed.* **2016**, *55*, 14067–14071; *Angew. Chem.* **2016**, *128*, 14273–14277; d) E. von Grotthuss, S. E. Prey, M. Bolte, H.-W. Lerner, M. Wagner, *Angew. Chem. Int. Ed.* **2018**, *57*, 16491–16495; *Angew. Chem.* **2018**, *130*, 16729–16733.
[7] J. W. Taylor, A. McSkimming, C. F. Guzman, W. H. Harman, *J. Am. Chem. Soc.* **2017**, *139*, 11032–11035.
[8] a) D. Wu, L. Kong, Y. Li, R. Ganguly, R. Kinjo, *Nat. Commun.* **2015**, *6*, 7340–7345; b) B. Wang, Y. Li, R. Ganguly, H. Hirao, R. Kinjo, *Nat. Commun.* **2016**, *7*, 11871–11880; c) Y. Su, Y. Li, R. Ganguly, R. Kinjo, *Angew. Chem. Int. Ed.* **2018**, *57*, 7846–7849; *Angew. Chem.* **2018**, *130*, 7972–7975.
[9] For a recent review, see: Y. Su, R. Kinjo, *Chem. Soc. Rev.* **2019**, *48*, 3613–3659.
[10] a) S. E. Prey, C. Herok, F. Fantuzzi, M. Bolte, H.-W. Lerner, B. Engels, M. Wagner, *Chem. Sci.* **2023**,*14*, 849–860; b) I. Cortés, J. Cabrera-Trujillo, I. Fernández, *ACS Org. Inorg. Au* **2022**, *2*, 44–52.
[11] a) I. Fernández, F. M. Bickelhaupt, *Chem. Soc. Rev.* **2014**, *43*, 4953–4967; b) L. P. Wolters, F. M. Bickelhaupt, *WIREs Comput. Mol. Sci.* **2015**, *5*, 324–343; c) F. M. Bickelhaupt, K. N. Houk, *Angew. Chem. Int. Ed.* **2017**, *56*,10070-10086; *Angew. Chem.* **2017**, *129*, 10204–10221. See also; d) I. Fernández, in Discovering the Future of Molecular Sciences (Ed.: B. Pignataro), Wiley-VCH, Weinheim, **2014**, pp. 165–187.
[12] For reviews on the EDA method, see: a) F. M. Bickelhaupt, E. J. Baerends, in *Reviews in Computational Chemistry*, (Eds. K. B. Lipkowitz, D. B. Boyd), Wiley-VCH: New York, **2000**, Vol. 15, pp. 1–86; b) M. von Hopffgarten, G. Frenking, *WIREs Comput. Mol. Sci.* **2012**, *2*, 43–62; c) I. Fernández, in *Applied Theoretical Organic Chemistry*, (Ed. D. J. Tantillo), World Scientific, New Jersey, 2018, pp. 191–226.
[13] Selected recent representative examples: a) D. N. Kamber, S. S. Nguyen, F. Liu, J. S. Briggs, H.-W. Shih, R. D. Row, Z. G. Long, K. N. Houk, Y. Liang, J. A. Prescher, *Chem. Sci.* **2019**, *10*, 9109–9114; b) A. Couce-Ríos, A. Lledós, I. Fernández, G. Ujaque, *ACS Catal.* **2019**, *9*, 848–858; c) I. Fernández, *Chem. Sci.* **2020**, *11*, 3769–3779; d) P. Vermeeren, T. A. Hamlin, I. Fernández, F. M. Bickelhaupt, *Angew. Chem. Int. Ed.* **2020**, *59*, 6201–6206; *Angew. Chem.* **2020**, *132*, 6260–6265; e) P. Vermeeren, T. A. Hamlin, I. Fernández, F. M. Bickelhaupt, *Chem. Sci.* **2020**, *11*, 8105–8112; f) T. A. Hamlin, F. M. Bickelhaupt, I. Fernández, *Acc. Chem. Res.* **2021**, *54*, 1972–1981; g) T. Hansen, P. Vermeeren, F. M. Bickelhaupt, T. A. Hamlin, *Angew. Chem. Int. Ed.* **2021**, *60*, 20840–20848; *Angew. Chem.* **2021**, *133*, 21008–21016; h) T. A. Hamlin, F. M. Bickelhaupt, I. Fernández, *Acc. Chem. Res.* **2021**, *54*, 1972–1981.
[14] a) D. Yepes, P. Jaque, I. Fernández, *Chem. Eur. J.* **2016**, *22*, 18801–18809; b) D. Yepes, P. Jaque, I. Fernández, *Chem. Eur. J.* **2018**, *24*, 8833–8840; c) J. J. Cabrera-Trujillo, I. Fernández, *Chem. Eur. J.* **2018**, *24*, 17823–17831; d) J. J. Cabrera-Trujillo, I. Fernández, *J. Phys. Chem. A* **2019**, *123*, 10095–10101; e) J. J. Cabrera-Trujillo, I. Fernández, *Inorg. Chem.* **2019**, *58*, 7828–7836; f) J. J. Cabrera-Trujillo, I. Fernández, *Chem. Eur. J.* **2021**, *27*, 3823–3831; g) J. J. Cabrera-Trujillo, I. Fernández, *Chem. Commun.* **2022**, *58*, 6801–6804.
[15] For a Feature article, see: I. Fernández, *Chem. Commun.* **2022**, *58*, 4931–4940.
[16] a) Y. García-Rodeja, F. M. Bickelhaupt, I. Fernández, *Chem. Eur. J.* **2016**, *22*, 13669–13676; b) B. Ghosh, J. J. Cabrera-Trujillo, I. Fernández, A. K. Phukan, *Inorg. Chem. Front.* **2022**, *9*, 5673–5687.
[17] M. P. Mitoraj, A. Michalak, T. Ziegler, *J. Chem. Theory Comput.* **2009**, *5*, 962–975.
[18] a) J. E. Leffler, *Science* **1953**, *117*, 340–341; b) G. S. A. Hammond, J . *Am. Chem.* **1955**, *77*, 334–338.
[19] Z. Chen, C. S. Wannere, C. Corminboeuf, R. Puchta, P. v. R. Schleyer, *Chem. Rev.* **2005**, *105*, 3842–3888.
[20] a) R. Herges, D. Geuenich, *J. Phys. Chem. A* **2001**, *105*, 3214–3220; b) D. Geuenich, K. Hess, F. Köhler, R. Herges, *Chem. Rev.* **2005**, *105*, 3758–3772.
[21] For a related aromaticity gain in anthracene derivatives, see: a) Y. García-Rodeja, I. Fernández, *Chem. Eur. J.* **2017**, *23*, 6634–6642; b) P. Izquierdo-García, J. M. Fernández-García, J. Perles, I. Fernández, N. Martín, *Angew. Chem. Int. Ed.* **2023**, *62*, e202215655; *Angew. Chem.* **2023**, *135*, e202215655.
[22] Performing this analysis at a consistent point along the reaction coordinate (near all transition structures), rather than the transition state alone, ensures that the results are not skewed by the position of the transition state.
[23] J. J. Cabrera-Trujillo, I. Fernández, *Chem. Commun.* **2019**, *55*, 675–678.
[24] Gaussian 09, Revision D.01, M. J. Frisch, G. W. Trucks, H. B. Schlegel, G. E. Scuseria, M. A. Robb, J. R. Cheeseman, G. Scalmani, V. Barone, G. A. Petersson, H. Nakatsuji, X. Li, M. Caricato, A. Marenich, J. Bloino, B. G. Janesko, R. Gomperts, B. Mennucci, H. P. Hratchian, J. V. Ortiz, A. F. Izmaylov, J. L. Sonnenberg, D. Williams-Young, F. Ding, F. Lipparini, F. Egidi, J. Goings, B. Peng, A. Petrone, T. Henderson, D. Ranasinghe, V. G. Zakrzewski, J. Gao, N. Rega, G. Zheng, W. Liang, M. Hada, M. Ehara, K. Toyota, R. Fukuda, J. Hasegawa, M. Ishida, T. Nakajima, Y. Honda, O. Kitao, H. Nakai, T. Vreven, K. Throssell, J. A. Montgomery, Jr., J. E. Peralta, F. Ogliaro, M. Bearpark, J. J. Heyd, E. Brothers, K. N. Kudin, V. N. Staroverov, T. Keith, R. Kobayashi, J. Normand, K. Raghavachari, A. Rendell, J. C. Burant, S. S. Iyengar, J. Tomasi, M. Cossi, J. M. Millam, M. Klene, C. Adamo, R. Cammi, J. W. Ochterski, R. L. Martin, K. Morokuma, O. Farkas, J. B. Foresman, and D. J. Fox, Gaussian, Inc., Wallingford CT, **2016**.
[25] a) A. D. Becke, *J. Chem. Phys.* **1993**, *98*, 5648–5652; b) C. Lee, W. Yang, R. G. Parr, *Phys. Rev. B* **1998**, *37*, 785–789; c) S. H. Vosko, L. Wilk, M. Nusair, *Can. J. Phys.* **1980**, *58*, 1200–1211.
[26] S. Grimme, J. Antony, S. Ehrlich, H. Krieg, *J. Chem. Phys.* **2010**, *132*, 154104–19.
[27] F. Weigend, R. Ahlrichs, *Phys. Chem. Chem. Phys.* **2005**, *7*, 3297–3305.
[28] a) S. Miertuš, E. Scrocco, J. Tomasi, *Chem. Phys.* **1981**, *55*, 117–129; b) J. L. Pascual-Ahuir, E. Silla, I. Tuñón, *J. Comput. Chem.* **1994**, *15*, 1127–1138; c) V. Barone, M. Cossi, *J. Phys. Chem. A* **1998**, *102*, 1995–2001.
[29] C. Gonzalez, H. B. Schlegel, *J. Phys. Chem.* **1990**, *94*, 5523–5527.
[30] Y. Zhao, D. G. Truhlar, *Theor. Chem. Acc.* **2008**, *120*, 215–241.
[31] K. Wolinski, J. F. Hilton, P. Pulay, *J. Am. Chem. Soc.* **1990**, *112*, 8251–8260.
[32] a) G. te Velde, F. M. Bickelhaupt, E. J. Baerends, C. Fonseca Guerra, S. J. A. van Gisbergen, J. G. Snijders, T. Ziegler, *J. Comput. Chem.* **2001**, *22*, 931–967; b) *ADF2020*, SCM, Theoretical Chemistry, Vrije Universiteit, Amsterdam, The Netherlands, http://www.scm.com.
[33] J. G. Snijders, P. Vernooijs, E. J. Baerends, *At. Data Nucl. Data Tables 198* **1**, *26*, 483–574.
[34] J. Krijn, E. J. Baerends, *Fit Functions in the HFS-Method*, Internal Report (in Dutch), Vrije Universiteit Amsterdam, The Netherlands, **1984**.
[35] a) E. van Lenthe, E. J. Baerends, J. G. Snijders, *J. Chem. Phys.* **1993**, *99*, 4597–4610; b) E. van Lenthe, E. J. Baerends, J. G. Snijders, *J. Chem. Phys.* **1994**, *101*, 9783–9792; c) E. van Lenthe, A. Ehlers, E. J. Baerends, *J. Chem. Phys.* **1999**, *110*, 8943–8953.

Manuscript received: February 21, 2023
Accepted manuscript online: April 6, 2023
Version of record online: April 27, 2023